

# COMPRESSIVE SPECTRAL IMAGING WITH COLORED-PATTERNED DETECTORS

Claudia V. Correa\*, Henry Arguello† and Gonzalo R. Arce\*

\*Dept. of Electrical and Computer Engineering, University of Delaware, Newark, Delaware, USA, 19716

†Dept. of Computer Science, Universidad Industrial de Santander, Bucaramanga, Colombia, 680002

E-mail: {clavicop,arce}@udel.edu, henarfu@uis.edu.co

## ABSTRACT

Compressive spectral imaging captures the spatial and spectral information of a scene using a set of two-dimensional random projections. Compressed sensing reconstruction algorithms are then used to recover the underlying three-dimensional source. This work presents a new generation of devices that attain compressive spectral image measurements by means of a colored-patterned detector and a dispersive element. Simulations show that these new generation devices can recover spectral scenes with up to 5 dB gain in PSNR with respect to traditional Coded Aperture Snapshot Spectral Imaging (CASSI) systems.

**Index Terms**— Colored patterned detectors, compressive spectral imaging, optical filters.

## 1. INTRODUCTION

Traditional spectral imaging sensors acquire large amounts of data, by scanning either the spatial or spectral coordinates to attain the underlying data cubes. The complexity thus grows linearly with the desired resolution. Compressive spectral imaging (CSI) devices, on the other hand, sense spatial and spectral information of a scene using 2-dimensional compressive measurements. CSI assumes that hyperspectral images have a sparse representation in a given basis. More specifically, a datacube  $\mathbf{F} \in \mathbb{R}^{N \times N \times L}$ , or its vectorized form  $\mathbf{f} \in \mathbb{R}^{N^2 L}$ , has a  $S$ -sparse representation in a basis  $\Psi$  if it can be represented as a linear combination of  $S \ll N^2 L$  vectors in  $\Psi$ . An architecture that attains CSI measurements is the Coded Aperture Snapshot Spectral Imaging (CASSI) system [1, 2]. Figure 1(a) depicts the CASSI architecture in which, a coded aperture pattern first encodes the information, and a dispersive element subsequently shears the coded source along the x-axis [3]. Compressive spectral imaging establishes that  $v \gtrsim S \log(N^2 L) \ll N^2 L$  random projections are sufficient to recover  $\mathbf{f}$  with high probability. CSI measurements can be modeled as  $\mathbf{g} = \mathbf{H}\mathbf{f}$ , where  $\mathbf{H}$  is the transfer function of the optical system. This matrix accounts for the effects of the optical elements in the device [4].

This research was supported by ONR under the contract N00014-10-C-0199.

To date, CSI devices have used traditional optical elements including focal plane array (FPA) detectors, and block-unblock coded aperture patterns. These patterns are masks that affect all wavelengths on each spatial location.

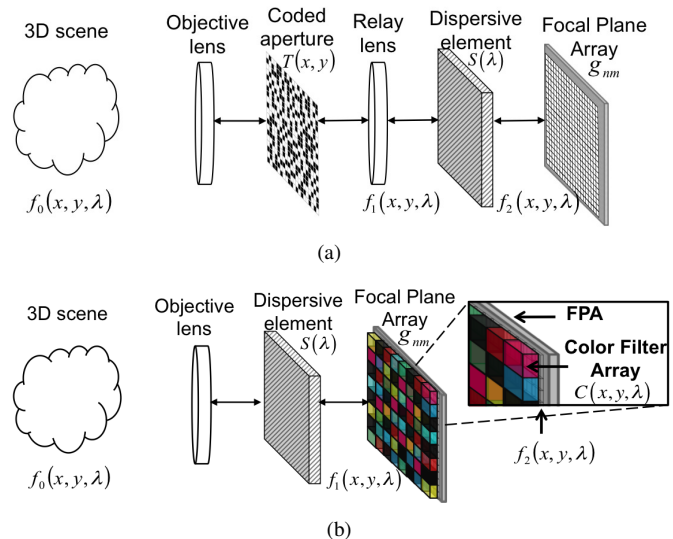


**Fig. 1.** Compressive spectral imaging architectures. (a) Coded aperture snapshot spectral imaging (CASSI) system and, (b) Compressive patterned snapshot imager (CPSI).

This work leverages a new generation of thin film devices which lead to improved spectral imaging systems. In particular, a Compressive Spectral Patterned Snapshot Imager (CSPSI) is introduced. As shown in Fig. 1(b), the system uses a colored-patterned FPA detector combined with a dispersive element, to capture the spatial and spectral information of a source in a snapshot. Unlike traditional irradiance sensors that capture the source uniformly across a range of wavelengths, patterned detectors are made of a tiling of optical filters with different spectral responses. Thus, each spatial coordinate samples the spectral data cube along different wavelengths.

Colored mosaic detectors have been used in imaging devices. For instance, the Bayer pattern [5] can be found in most solid-state color cameras. Snapshot multispectral cam-

eras based on patterned detector technology [6, 7, 8] have been recently developed. These architectures capture the information over a few spectral bands but since each pixel is assigned a single color, there is a trade off between spatial and spectral resolution, which is the main drawback of these designs. Another architecture for multispectral imaging using color filter arrays is presented in [9]. This architecture however, requires four sensors to capture the spatial and spectral information in a scene.

The new CPSI architecture proposed here exploits the theory of compressed sensing, and thus improves the spatial and spectral resolution in the reconstructed images. In general, when color filter arrays are used as the principal sensing device, the resolution of the images are limited by the number of colors in the detector array. In contrast, the combination of color filter arrays and a dispersive element increases the attainable spectral and spatial resolution. Since coded apertures are no longer needed in CPSI, due to the embedded coding in the patterned detector elements, the new imager is considerably simpler. In the following sections, the discretization model of the compressive spectral imager with colored-patterned detectors is developed. The forward model in matrix notation is presented. Simulations and results are included to analyze the performance of CPSI with respect to the traditional CASSI system. Simulations assume ideal negligible transition bands of the optical filters.

## 2. COMPRESSIVE SPECTRAL IMAGING WITH COLORED PATTERNED DETECTORS

### 2.1. Discretization of The Mathematical Model

CPSI exploits colored-patterned detectors along with computational imaging. Figure 1(b) depicts the CPSI architecture where the source is first dispersed by a prism and then spectrally filtered by the coded elements in the detector. Denote the analog 3D spatio-spectral source density as  $f_0(x, y, \lambda)$ , where  $(x, y)$  index the spatial coordinates and  $\lambda$  indexes the spectral components. The spectral dispersion of the source yields

$$f_1(x, y, \lambda) = \iint f_0(x', y', \lambda) h(x' - x, y' - y - S(\lambda)) dx' dy', \quad (1)$$

where  $S(\lambda)$  represents the dispersion and  $h$  is the impulse response of the system. The field  $f_1(x, y, \lambda)$  is then coded by the color filter array in the FPA detector  $C(x, y, \lambda)$ , resulting in

$$f_2(x, y, \lambda) = f_1(x, y, \lambda) C(x, y, \lambda). \quad (2)$$

Finally, the output of the system, denoted as  $g(x, y)$ , is obtained by integrating the field  $f_2(x, y, \lambda)$  over the spectral range sensitivity of the detector  $\Lambda$

$$g(x, y) = \int_{\Lambda} f_2(x, y, \lambda) d\lambda. \quad (3)$$

The energy captured in the  $(n, m)$ th pixel is represented by

$$g_{m,n} = \iint g(x, y) p(m, n; x, y) dx dy, \quad (4)$$

where  $p(m, n; x, y) = \text{rect}\left(\frac{x}{\Delta} - m, \frac{y}{\Delta} - n\right)$  corresponds to the discretization of the  $(m, n)$ th pixel, and  $\Delta$  is the pixel pitch. The discretization of the analog spatio-spectral source is obtained by calculating the energy on each voxel of the datacube  $f_{m,n,k}$ . The discrete representation of the scene can be obtained by

$$f_{m,n,k} = \int_{\lambda_k}^{\lambda_{k+1}} \int_{n\Delta}^{(n+1)\Delta} \int_{m\Delta}^{(m+1)\Delta} f_0(x, y, \lambda) dx dy d\lambda, \quad (5)$$

where  $m, n$  are the discrete indices for spatial coordinates and  $k$  is the discrete index for the spectral components. The discretization in (5) provides a data cube with  $N \times N$  spatial resolution and  $L$  spectral bands. Notice that the width of each band is determined by the dispersion function of the prism  $S(\lambda)$ . The discrete representation of the color filter array on the FPA,  $C(x, y, \lambda)$ , has the same pixel pitch as that of the detector, such that each element of the detector matches exactly one element of the filter array.  $C(x, y, \lambda)$  can be thus expressed as

$$C(x, y, \lambda) = \sum_{m,n,k} C_{m,n,k} \text{rect}\left(\frac{x}{\Delta} - m, \frac{y}{\Delta} - n, \frac{\lambda}{\Delta} - k\right). \quad (6)$$

Figure 2 shows a zoomed version of a source voxel after it is sheared by the dispersive element. There, the dispersion function  $S(\lambda)$  causes the energy from a single voxel to be mapped onto three detector pixels, such that each source voxel can be split into three regions  $R_0, R_1$  and  $R_2$ . The corresponding energy of each region impinges in three different detector elements with energy indexed by the weights  $w_{m,n,k,u}$  [10], where  $m, n$  index the spatial coordinates,  $k$  indexes the spectral dimension and  $u$  accounts for the region  $R_0, R_1$  or  $R_2$ . More specifically,  $w_{m,n,k,u} = (f_{m,n,k})^{-1} \int \int \int_{R_u} dx dy d\lambda$ . Notice that Fig. 2 shows the shearing operation of a voxel before it passes through the color filter array. Using the previous discrete representations, and assuming ideal PSF of the lens, Eq. (4) becomes the discrete output written as

$$g_{m,n} = \sum_{k=0}^{L-1} \sum_{u=0}^2 w_{m,n,k,u} f_{m,(n-k-u),k} C_{m,n,k}, \quad (7)$$

resulting in a  $N \times V$  measurement set with  $V = N + L + 1$ .

The proportion of energy that passes through the color filter array, known as the transmittance, can be calculated as  $Tr = \sum_{m,n,k} C_{m,n,k} / (NVL)$ , where ideal optical filters with

negligible transition bands are assumed.

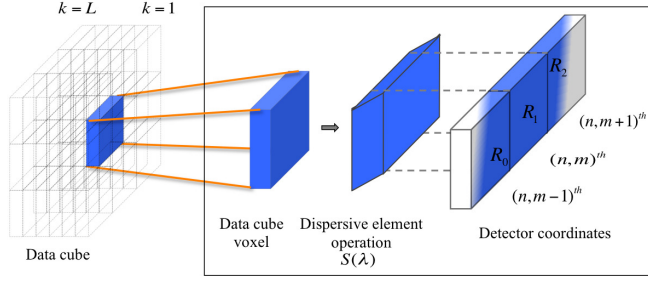


**Fig. 2.** Zoomed version of a source voxel being dispersed and measured. After the dispersive element, the sheared voxel impinges onto three neighboring detector elements.

## 2.2. Matrix Model

Let  $\mathbf{g}$  be the vectorized representation of the measurements  $g_{m,n}$  in (7). The compressive spectral imager with colored patterned detectors can be modeled as

$$\mathbf{g} = \mathbf{H}\mathbf{f}, \quad (8)$$

where  $\mathbf{f} \in \mathbb{R}^{N^2L}$  is the vectorized representation of the source in (5), and  $\mathbf{H}$  is a  $NV \times N^2L$  matrix representing the optical system transfer function. The matrix  $\mathbf{H}$  is determined by the spectral response of the color filter array, and its structure is intended to represent the dispersive element operation. More specifically, the entries of the  $m$ th row in the matrix  $\mathbf{H}$  are given by

$$(\mathbf{h}_m)_n = \begin{cases} \sum_{u=0}^2 (\mathbf{w}_k^u)_{m-(u+k)N} (\mathbf{c}_k)_{m-uN}, & \text{if } n-kN'+uN=m \\ 0, & \text{otherwise,} \end{cases} \quad (9)$$

for  $m = 0, \dots, NV - 1$ , and  $n = 0, \dots, N^2L - 1$ , with  $k = \lfloor n/N^2 \rfloor$ ; and  $N' = N^2 - N$ . The vectorized form of the weight values for region  $u$  in the band  $k$  is given by  $\mathbf{w}_k^u$ , and  $\mathbf{c}_k$  is a vector that represents the entries of the color filter array for the  $k$ th spectral band. Thus,  $(\mathbf{w}_k^u)_{m+nN} = w_{m,n,k,u}$  for  $m, n = 0, \dots, N-1$ ; and  $(\mathbf{c}_k)_{m+nN+kNV} = \mathbf{C}_{m,n,k}$  for  $m = 0, \dots, N-1$ ;  $n = 0, \dots, V-1$ ; and  $k = 0, \dots, L-1$ .

Figure 3 depicts the matrix  $\mathbf{H}$  for  $N = 6$ ,  $L = 3$ . It can be noticed that  $\mathbf{H}$  is a highly structured and sparse matrix. The entries of the color filter array are arranged in three diagonals representing the vectors  $\mathbf{w}_k^0$ ,  $\mathbf{w}_k^1$ , and  $\mathbf{w}_k^2$ . Different color intensities represent different values of weights for each region.

## 3. SIMULATIONS AND RESULTS

A test data cube  $\mathbf{f}$  with spatial resolution of  $256 \times 256$  pixels and  $L = 8$  spectral bands in the range of 450nm to 620nm was

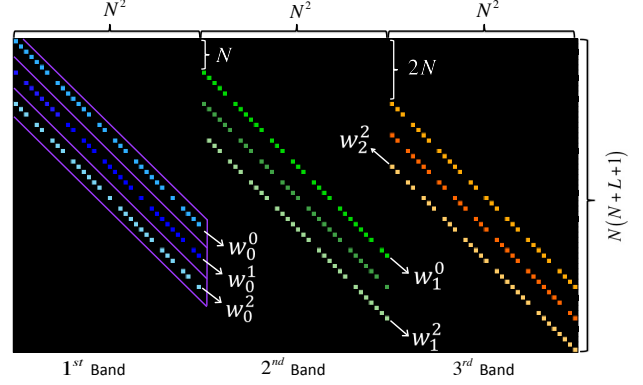


**Fig. 3.** Example of the sensing matrix  $\mathbf{H}$  for  $N = 6$  and  $L = 3$  using randomly generated colored optical filters. The colored squares represent the weights  $w_{n,m,k,u}$ .

used to analyze the performance of the proposed architecture. Figure 4 shows selected spectral bands of the test data cube and their center frequencies. Here, it is assumed that the frequency responses of the filters match the spectral channels of the test data cube. The colored patterns in the detector were obtained by randomly tiling a set of different filters with 50% transmittance. Simulations were performed varying the total number of color filters. Two types of patterns were used, the first one being combination of low pass and high pass (LHP) filters, and the second consisting of band pass (BP) filters. The central wavelength and bandwidth of the frequency responses were randomly generated.

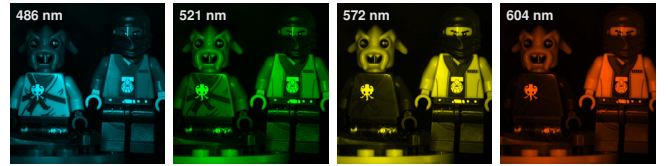


**Fig. 4.** Selected spectral bands of the test data cube. Each spectral slice has a spatial resolution of  $256 \times 256$  pixels.

Given the set of compressive measurements in (7) and, the color filter array in (6), reconstructions of the data cube were obtained using the GPSR algorithm [11]. This algorithm obtains a sparse representation of the source by solving the optimization problem  $\hat{\mathbf{f}} = \Psi \{ \arg \min_{\theta} \| \mathbf{g} - \mathbf{H}\Psi\theta \|_2 + \tau \| \theta \|_1 \}$ , where  $\tau$  is a regularization constant, and  $\Psi$  is the sparse representation basis that has been set as the Kronecker product between a 2D-Wavelet Symmlet 8 basis and the Discrete Cosine Transform. The results are compared with reconstructions obtained from the most recent model of the CASSI system presented in [10] using a single shot. In the CASSI system, the entries of the coded aperture are realizations of a Bernoulli random variable with parameter  $p = 0.5$ . Figure 5 shows

a comparison between the reconstructions obtained with the CPSI and the CASSI. It can be observed that the CPSI system provides higher accuracy in the reconstructions with an improvement of 5 dB in PSNR. In addition, Fig. 6 shows a zoomed version of the reconstruction of the 5th spectral band (521 nm). It can be seen that the CPSI system provides more details in the reconstructions. Also, the spectral reconstruction for three different points in the data cube is shown in Fig. 7. It can be seen that CPSI provides more accurate approximations of the spectral information of the source than the traditional CASSI. Figure 8 shows the mean reconstruction PSNR for the proposed architecture as a function of the number of colors in the filter array. Results show that the reconstruction quality increases with the number of colors. LHP and BP filters provide similar results.

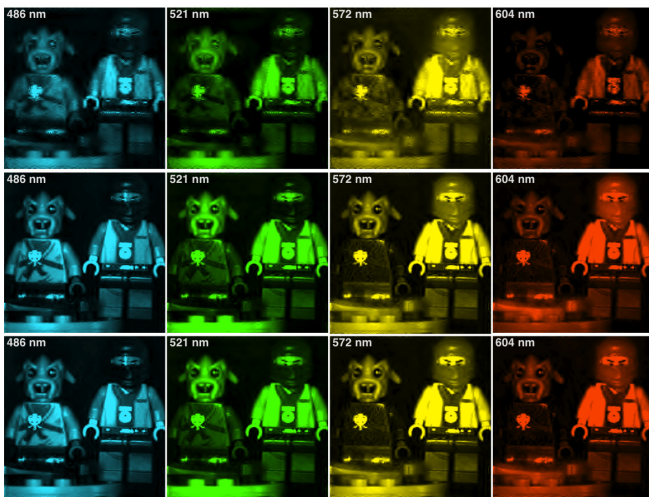


**Fig. 5.** Reconstructions of the spectral bands in Fig. 4 using (Top row) Single shot CASSI system, (PSNR 21.2 dB), (Middle row) colored patterned detector with 6 distinct LHP filters, (PSNR 26.46 dB) and, (Bottom row) colored patterned detector with 6 distinct BP filters, (PSNR 26.62 dB).



**Fig. 6.** Zoomed version of the reconstruction for the 5th spectral band using (Left) CASSI system, and (Right) colored patterned detector with 6 BP filters.

#### 4. CONCLUSIONS

A new generation of compressive snapshot spectral imaging devices has been introduced. The new CPSI system uses a

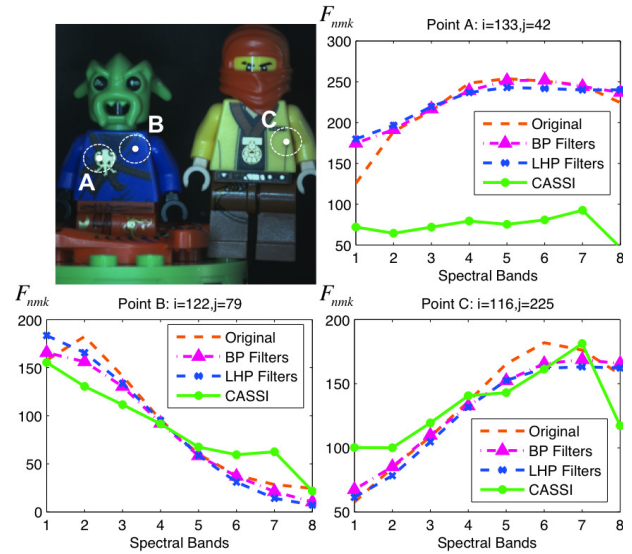


**Fig. 7.** Reconstruction along the spectral axis of the highlighted spatial pixel locations using CASSI, and CPSI with 6 BP and 6 LHP filters. Spectral responses for (Top-right) Point A; (Bottom-left) Point B; (Bottom-right) Point C.

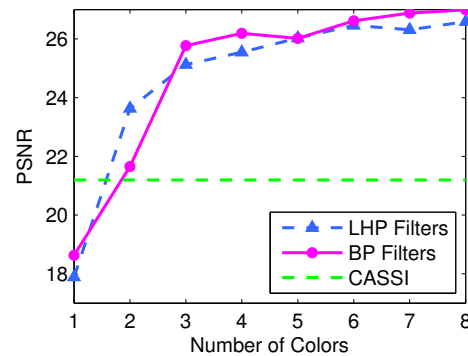


**Fig. 8.** Average reconstruction PSNR as a function of the number of colors in the patterned detector. Combinations of low-pass and high-pass (LHP) filters and, band-pass (BP) filters were used.

color patterned filter array in conjunction with an irradiance detector instead of the coded aperture used in CASSI. The proposed design exhibits less hardware complexity due to the patterned detector array. At the same time, the CPSI system exploits the advantages of compressive spectral imaging to capture hyperspectral scenes. The reconstruction PSNR is improved by about 5 dB when compared to the CASSI system, a better approximation of the spectral information and more level of spatial detail are attained in the reconstructions with the new architecture.

## 5. REFERENCES

- [1] A. A. Wagadarikar, R. John, R. Willett, and D. Brady, "Single disperser design for coded aperture snapshot spectral imaging," *Appl. Opt.*, vol. 47, pp. B44–B51, 2008.
- [2] H. Arguello and G. R. Arce, "Code aperture optimization for spectrally agile compressive imaging," *J. Opt. Soc. Am. A*, vol. 28, no. 11, pp. 2400–2413, November 2011.
- [3] H. Arguello and G. R. Arce, "Rank minimization code aperture design for spectrally selective compressive imaging," *IEEE Trans. Image Processing*, vol. 22, no. 3, pp. 941 – 954, 2013.
- [4] G. R. Arce, D. Brady, L. Carin, H. Arguello, and D. Kittle, "An introduction to compressive coded aperture spectral imaging," *Signal Processing Magazine, IEEE*, vol. 31, no. 1, pp. 105 – 115, 2014.
- [5] Bayer B.E., "Color imaging array," *US Patent 3,971,065*, July 1976.
- [6] B. Geelen, M. Jayapala, N. Tack, and A. Lambrechts, "Low-complexity image processing for a high-throughput low-latency snapshot multispectral imager with integrated tiled filters," *Proc. SPIE*, vol. 8743, pp. 87431E–87431E–13, 2013.
- [7] J. M. Eichenholz and J. Dougherty, "Ultracompact fully integrated megapixel multispectral imager," *Proc. SPIE*, vol. 7218, pp. 721814–1 – 721814–10, 2009.
- [8] J. M. Eichenholz, N. Barnett, Y. Juang, D. Fish, S. Spano, E. Lindsley, and D. L. Farkas, "Real time megapixel multispectral bioimaging," *Proc. SPIE*, vol. 7568, pp. 75681L–75681L–10, 2010.
- [9] Y. Murakami, M. Yamaguchi, and N. Ohya, "Hybrid-resolution multispectral imaging using color filter array," *Optics Express*, vol. 20, no. 7, pp. 7173–7183, 2012.
- [10] H. Arguello, H. Rueda, Y. Wu, D. W. Prather, and G. R. Arce, "Higher-order computational model for coded aperture spectral imaging," *Appl. Optics*, vol. 52, no. 52, pp. D12 – D21, 2013.
- [11] M. Figueiredo, R. Nowak, and S. Wright, "Gradient projection for sparse reconstruction: Application to compressed sensing and other inverse problems," *IEEE J. of Selected Topics in Signal Processing*, vol. 1, no. 4, pp. 586–597, 2007.